



Solid-state ultrasonic spot welding of SiCp/2009Al composite sheets



V.K. Patel^{a,*}, S.D. Bhole^a, D.L. Chen^a, D.R. Ni^b, B.L. Xiao^b, Z.Y. Ma^{b,*}

^a Department of Mechanical and Industrial Engineering, Ryerson University, 350 Victoria Street, Toronto, Ontario M5B 2K3, Canada

^b Shenyang National Laboratory for Materials Science, Institute of Metal Research, Chinese Academy of Sciences, 72 Wenhua Road, Shenyang 110016, China

ARTICLE INFO

Article history:

Received 31 July 2014

Accepted 17 September 2014

Available online 28 September 2014

Keywords:

Welding and joining

Particle-reinforced composites

Aluminum

Welding

Vibration

Microstructure

ABSTRACT

It has been challenging to join aluminum matrix composites (AMCs) using conventional fusion welding processes due to the occurrence of segregation and deleterious reactions between the reinforcement particles and liquid aluminum in the fusion zone. Development of robust welding processes to join AMCs thus holds the key in advanced lightweighting structural applications in the transportation sectors. The purpose of this study was to explore the weldability of AMCs via a solid-state welding technique – ultrasonic spot welding (USW). In this study 1.5 mm thick 17 vol.% SiCp/2009Al composite sheets in the annealing (O) and T6 conditions were subjected to USW, respectively, with the aim to demonstrate the welding feasibility of the composites. Microstructure, X-ray diffraction, microhardness and lap shear tensile tests were performed to evaluate the weld zone (WZ) characteristics in the USW joints. A characteristic band consisting of finer and denser crushed SiC particles that were uniformly embedded in the aluminum matrix was observed to occur in the WZ. The WZ of both types of joints had a much higher hardness than that of their respective base metal. The lap shear tensile fracture load increased with increasing welding energy and satisfied the requirement of AWS standard D17.2 for spot welding.

© 2014 Elsevier Ltd. All rights reserved.

1. Introduction

Particle reinforced aluminum matrix composites (AMCs) are a major focus of attention in aerospace, motor sport and automotive industrial fields due to their several attractive advantages over unreinforced alloys, such as high specific stiffness and strength at room or elevated temperatures, excellent wear resistance, excellent fatigue properties, high formability, and attractive thermal and electrical characteristics [1–3]. For the particle reinforcements, silicon carbide particle (SiCp) is an attractive reinforcement because of its low density, high wear, and oxidation resistances. Thus, SiCp reinforced Al matrix composites can offer potentially higher specific strength and stiffness. However, one of the main limitations for the industrial application of the particulate reinforced Al matrix composites is the difficulty in using conventional fusion welding methods because of the occurrence of the segregation of the reinforcement and deleterious reactions between the reinforcement particles and liquid Al in the fusion zone [2,4]. Previous studies showed that the high temperatures locally reached in the fusion zone during welding strongly promote the SiC–Al interface reaction given below [5,6]:



which deteriorated the mechanical and corrosion properties and of the joints [5,6]. Joint efficiency values attained in arc welding even with a careful choice of the filler material is seldom higher than 70% [6,7]. Thus, recently special attention has been paid to solid-state welding processes, namely friction stir/spot welding (FSW/FSSW), because the liquid phase reaction in the fusion zone can be avoided. However, Wang et al. [8] reported that the FSW joints of AMCs exhibited the lowest hardness in the heat-affected zone (HAZ) owing to the dissolution and coarsening of the precipitates during FSW, resulting in that the FSW AMCs joints usually failed in the HAZ. Therefore, the strength of the joints is usually determined by the hardness of the low-hardness zone of the HAZ.

Another solid-state welding technique is ultrasonic spot welding (USW), which produces coalescence via a simultaneous application of localized high-frequency vibratory energy and moderate clamping forces. USW process produces a very small HAZ [9,10], thus the earlier problem found in FSW/FSSW process can be avoided with this technique. In comparison with FSSW, USW has been shown to have a shorter weld cycle (typically < 0.4 s) and produce high quality joints that are stronger than FSSW when compared on the basis of the same nugget area [11,12].

So far no literatures on the USW of SiC/Al composites were reported, and thus, it is unclear how the SiC particles behave under the high frequency vibration and whether a sound spot joint of

* Corresponding authors. Tel.: +1 (416) 979 5000x4500 (V.K. Patel). Tel./fax: +86 24 83978908 (Z.Y. Ma).

E-mail addresses: vikas.patel@ryerson.ca (V.K. Patel), zym@imr.ac.cn (Z.Y. Ma).

these composites could be obtained via USW or not. This study was, therefore, aimed to identify the feasibility of joining a SiCp/2009Al sheet by USW process.

2. Materials and experimental procedure

In the present work, 2009Al (composition in wt.-%: 4.0Cu, 1.5Mg and balance Al) with an average size of 50 μm was selected for matrix. SiC particles with an average particle size of 7 μm were adopted as reinforcements. 1.5 mm thick sheets of 17 vol.-% SiC/2009Al under annealing (SiCp/2009Al-O) and T6 (SiCp/2009Al-T6) conditions were used for USW. For the 2009Al-T6 samples, a full annealed process was done while for the 2009Al-O samples, solution heat treatment was done at 515 $^{\circ}\text{C}$ for 1 h, then quenched under water and later aged at 175 $^{\circ}\text{C}$ for 6 h. The specimens of 80 mm long and 15 mm wide were sheared, with the faying surfaces ground using 120 emery paper, and then washed using acetone followed by ethanol and dried before welding. The welding was done with a dual wedge-reed Sonobond-MH2016 HP-USW system (schematic diagram shown in Fig. 1(a)) with rectangular 8 \times 6 mm welding tips. The samples were welded at an energy input ranging from 500 to 2000 J at a constant power setting of 2000 W, an impedance setting of 8 on the machine and a pressure of 0.414 MPa. To achieve 500–2000 J energy inputs, the USW procedure took 0.25–1 s. Cross-sectional samples for scanning electron microscopy (SEM) were polished using diamond paste and MasterPrep. X-ray diffraction (XRD) was carried out on fracture surfaces after tensile shear tests, using Cu K α radiation at 45 kV and 40 mA. The diffraction angle (2θ) at which the X-rays hit the samples varied from 20 $^{\circ}$ to 100 $^{\circ}$ with a step size of 0.05 $^{\circ}$ and 2 s in each step. A computerized Buehler microhardness testing machine was used for the micro-indentation hardness tests diagonally across the welded joints using a load of 500 g for 15 s. The distance between two successive hardness measurement was 0.5 mm. Tensile shear tests of the welds were conducted to measure the lap-shear failure load using a fully computerized United testing machine with a constant crosshead speed of 1 mm min $^{-1}$ in air at room temperature. In the tensile lap shear testing, restraining shims or spacers were used to minimize the rotation of the joints and maintain the shear loading as long as possible (Fig. 1(b)).

3. Results and discussion

3.1. Microstructure

Figs. 2(a) and 3(a) show the overall micrographs of the similar USWed SiCp/2009Al-O and SiCp/2009Al-T6 joints produced by 2000 J energy input, respectively. Since the highest lap shear tensile fracture load was observed at 2000 J (shown later in Section 3.4) for both joints (USWed SiCp/2009Al-O and SiCp/2009Al-T6 joints), USW samples welded with 2000 J energy inputs, were used for detail examination of their microstructure. It can be seen from the center of the welded joint shown Figs. 2(b) and 3(b) that no defects such as a porosity or cluster of SiC particles were observed in the joints, which are prone in the fusion welding of AMCs, indicating that a sound joint could be achieved by USW at 2000 J energy input. Moreover, no indication of the presence of visible brittle phases in the weld nugget, such as Al $_4$ C $_3$ phase that forms in conventional fusion welding method, was detected [13,14]. Similar, sound joints were also produced with energy inputs of 500, 1000, and 1500 J (not shown). By observing the Figs. 2(b) and 3(b), it can be seen that the weld zones (WZ) in both the USWed SiCp/2009Al-O and USWed SiCp/2009Al-T6 joints showed a band like microstructure. To show the clear difference

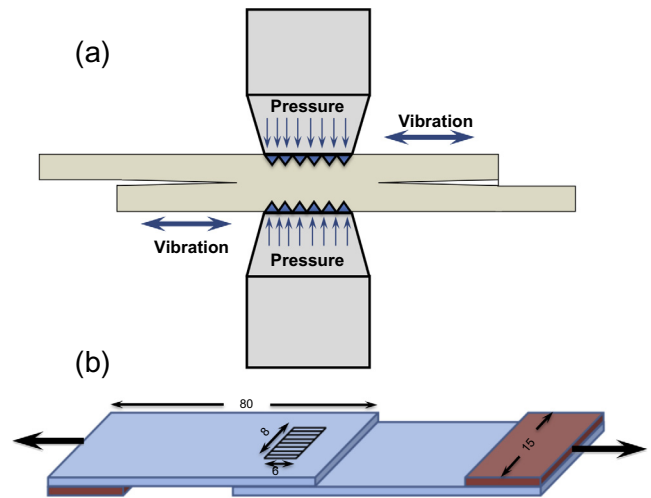


Fig. 1. Schematic diagrams of (a) USW process, (b) a 3D view of the lap shear tensile test specimen (mm).

between the two regions (WZ and BM), region c and d in Figs. 2(b) and 3(b) were magnified and shown in Figs. 2(c), (d) and 3(c), (d), respectively. However, from the magnified images shown in Fig. 2(c) and (d) of USWed SiC/2009Al-O samples, there was not clear difference found between WZ and upper/bottom region of the WZ. Thus, Fig. 2(c) and (d) further magnified and shown in (e) and (f), respectively. From these Figs. 2(e), (f) and 3(c), (d), it suggested that the plasticized composite is subjected to severe shear strain rate caused by the high frequency vibration energy. Some of the interesting observations were identified from Figs. 2(e), (f) and 3(c), (d), which are listed below,

- Observation 1. In both USWed samples, WZ regions contained higher volume fractions of SiC particles compare to the BM (or top and bottom of the WZ) (Figs. 2(e), (f) and 3(c), (d)).
- Observation 2. The band like structure thickness in USWed T6 sample was approximately only $\sim 60 \mu\text{m}$ (Fig. 3(b)), while it was around $\sim 1000 \mu\text{m}$ in that of the USWed O condition sample (Fig. 2(b)).
- Observation 3. By observing Figs. 2(f) and 3(d), it was found that after the USW process, the size of the SiC particles in O condition sample remained almost similar like BM ($\sim 7 \mu\text{m}$), while in T6 condition sample, it decreased and became around $\sim 2 \mu\text{m}$.

In order to understand the phenomenon of these three observations, the schematic diagram of the SiCp/Al composite sheet under the process of USW was drawn and shown in Fig. 4. In the first stage, two AMCs sheets comes in the contact with normal sonotrode compressive force (Fig. 1(a)), and the oxide film on the surface of SiCp/2009Al samples was destroyed. This compressive force brings direct contact of AMCs-to-AMCs. In the second stage, the high ultrasonic vibration under the action of high shear force produces greater level of friction, which leads to higher temperature at the center of the weld interface within as low as 0.5 s (close to the melting point, from our previous experiments [15]). The higher temperature at the weld interface during USW also reported by Elangovan et al., where the relationship between temperature and sample thickness with FEM based study is shown [16]. Because of higher temperature at weld interface, Al-matrix near the interface experienced semi-liquid state and becomes softer, and tries to squeezed away from the WZ. Eventually, WZ left with higher volume fraction of hard SiC particles with less amount of Al matrix (Observation 1). The interesting factor of the squeezed away

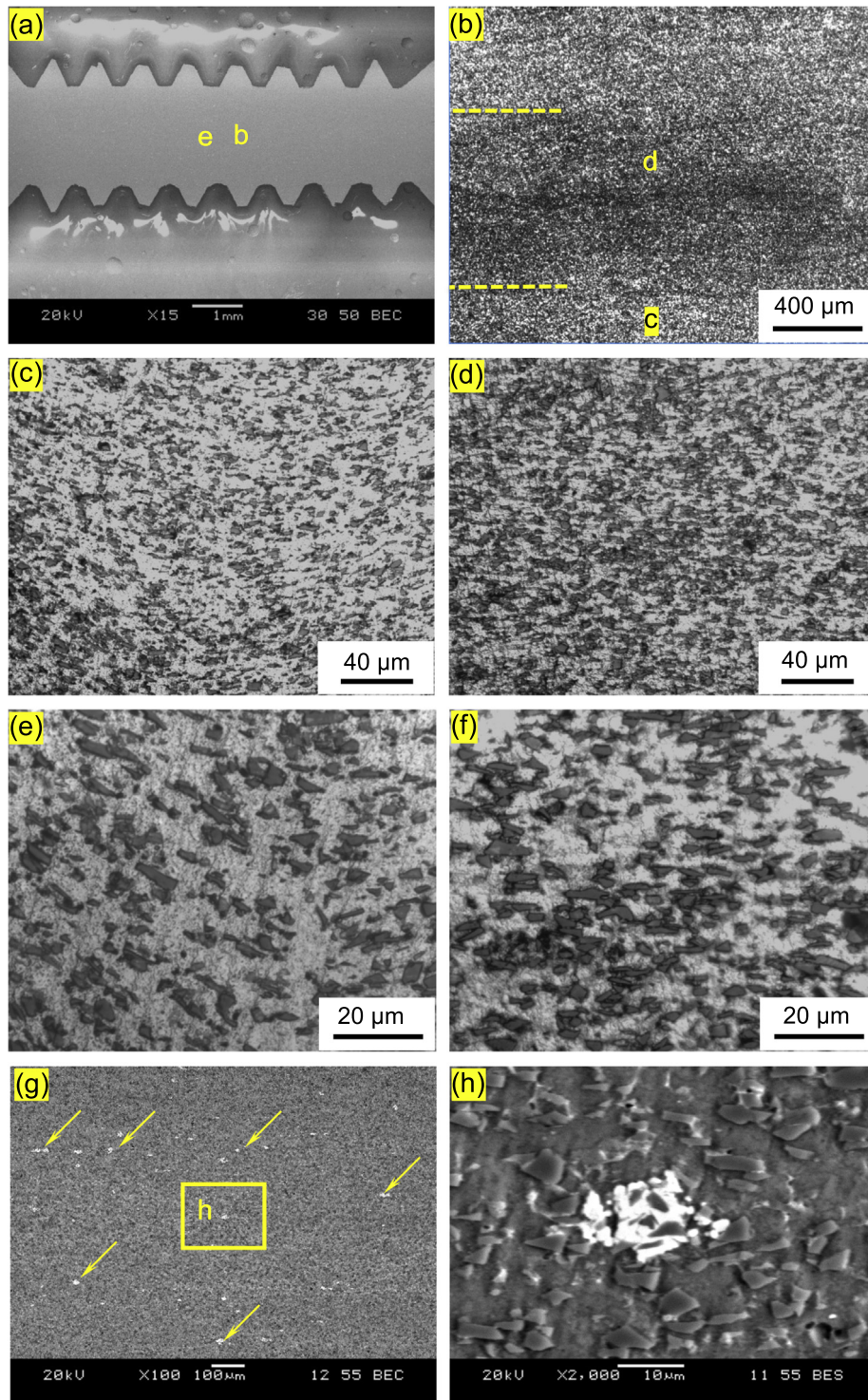


Fig. 2. SEM micrograph of USWed SiCp/2009Al–O using 2000 J welding energy (a) overall image of mounted USW joints, (b) magnified image of region b in (a), (c) OM image of magnified region of c in (b), (d) magnified image of region d in (b) showing band like structure, (e) further magnified images of region e in (a), (f) magnified SEM micrograph of region f in (e), (g) micrograph at the center of joints showing precipitated θ (Al_2Cu) phase, and (h) further magnified image of region h in (g).

direction of softer Al matrix shown in Fig. 4(b) and (c) answered the enormous difference between the band thickness in O and T6 condition as described earlier. In the USWed SiCp/2009Al–O, as seen from Fig. 4(b), semi-liquid Al-matrix can be flow in the upward and linear direction, since the Al matrix is softer in WZ due to the higher temperature and even also softer in BM region because of O condition. While, in T6 condition, the flow of the semi-liquid Al matrix can be stopped in upward direction by the

hard Al matrix of BM (due to T6 condition), Thus Al-matrix can only linearly travel and squeezed away from the weld interface. Therefore, USWed SiCp/2009Al–T6 sample left with the smaller band in compare to the that in USWed SiCp/2009Al–O sample (Observation 2). In this smaller band region in T6 condition, SiC particles start to vibrate against each other (in the action of shear direction) and generates crushing powder/smaller SiC particles of $\sim 2 \mu\text{m}$ (Fig. 3(d)). While in O condition, SiC particles can easily

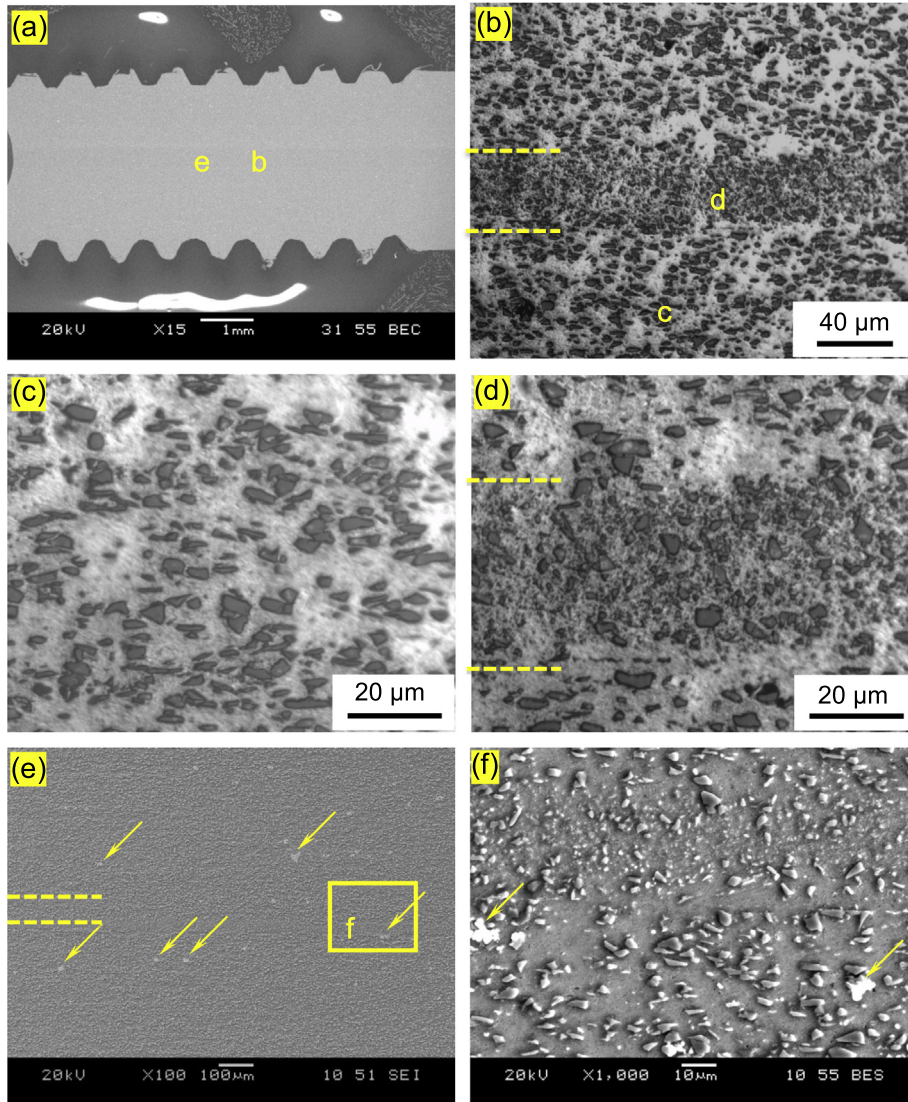


Fig. 3. SEM micrograph of the USWed SiCp/2009Al-T6 joint using 2000 J welding energy (a) overall image of USW joints, (b) magnified image of region b in (a), (c) OM image of magnified region of c in (b), (d) magnified image of region d in (b) showing band like structure, (e) micrograph at the center of the welded joints which shows the precipitated θ (Al_2Cu) phase, and (f) further magnified image of region f in (e).

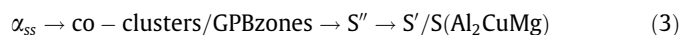
float in softer Al-matrix. Thus, the size of SiC particle remains unchanged ($\sim 7 \mu\text{m}$) (Fig. 2(f)) in USWed O condition (Observation 3).

The yellow arrows shown in Figs. 2(h) and 3(f) are representing the particles of Al_2Cu , which is identified by the energy-dispersive X-ray spectroscopy (EDS) and XRD (shown later). The EDS point analysis was performed on the white particle shown Figs. 1(h) and 3(f). The EDS point analysis result USWed O and T6 condition samples show 71.4% Al, 24.3% Cu, and 4.32% Si (in at.%) and 69.4% Al, 23.3% Cu, and 7.3% Si (in at.%). From this it is indicated that Al_2Cu phase formed during the annealing (O) and artificial aging in T6 conditions.

3.2. X-ray diffractions

To further verify the above microstructural observations, XRD data obtained on the BM and fracture surfaces of the USW joint are shown in Fig. 5(a) and (b), respectively. Apart from the Al and SiC peaks, Al_2Cu (θ) intermetallic phase was identified on the both BM and fracture surfaces of both samples. The present of

the θ phase in XRD result is in agreement with the SEM/EDS point analysis observation shown in Figs. 2(h) and 3(f). This θ phase was precipitated during the annealing and T6 process. The recent study of Wang et al. [8] on FSWed 2009Al/SiC (not annealed or T6 condition) showed that, along with the θ phase, S (Al_2CuMg) was also observed after the FSW process in the stir zone. This S phase was also observed by Bozkurt et al. [5] of FSWed AA2124-T4/SiC composite. However, The XRD pattern (Fig. 5) shows no evidence of present of S phase. It could be beyond the detection limits of XRD due to small volume fraction of it. The precipitation sequence of Al-Cu-Mg alloy could become very complex depending on the Cu/Mg ratio. Two-precipitation sequence (Al-Cu and Al-Cu-Mg alloys) could be overlapped, which would complicate the estimation of hardening behavior [18]:



The θ phase appears with high Cu/Mg ratio, while S phase appears with low Cu/Mg ratio in Al-Cu-Mg alloy [17]. Other phases such as a Al-C phase was also not found. Thus, it can say that unlike

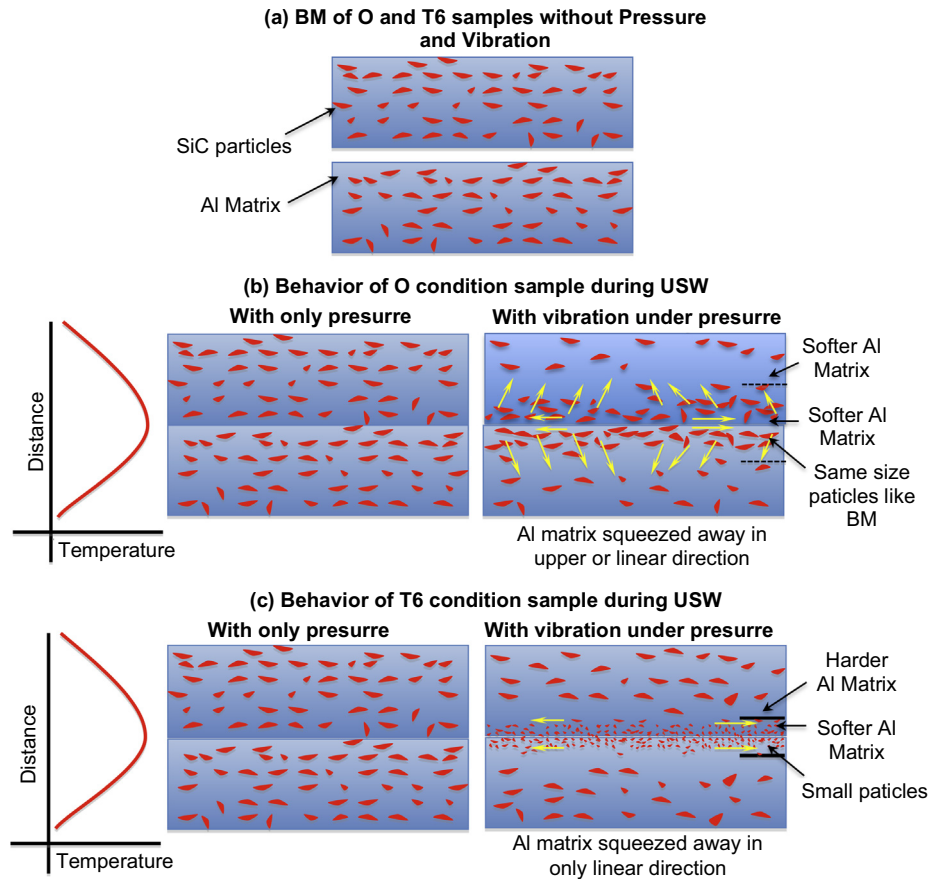


Fig. 4. Schematic diagram of the effect of high frequency vibration energy on the SiCp/Al composite sample during the USW process.

fusion welding, the frictional heat generated during USW did not promote any reaction between the Al matrix and SiC particle, however, as said earlier it could be beyond the detection limits of XRD.

3.3. Microhardness

The hardness profile diagonally across the center of the welded joints are shown in Fig. 6(a). In the annealing sample, in both 1000 and 2000 J energy inputs, the average microhardness on the top and bottom of the specimens were around 80 HV, which is similar to that in the BM. On the other hand, the microhardness of the WZ was higher than that of the BM. The average microhardness in the WZ for 1000 and 2000 J energy input specimens were approximately 100 and 150 HV, respectively. The higher hardness in the WZ is attributed to the number of reasons. First, as mentioned in the microstructure section, softer Al is being squeezed off from the WZ during the USW process and WZ left with higher density of small SiC particle, which inhibit the materials flow/dislocation movement and makes higher hardness. Second, the debris of fragmented particles will act as nucleation sites leading to grain refinement. This reduction of the grain size due to the recrystallization during USW could also involve in the enhancement of the hardness in the WZ. Recrystallization during USW was observed previously in the literatures [15,18]. Third, from the equation of dislocation density express as,

$$\rho = 12 \frac{\Delta\alpha\Delta Tf}{b(2r)(1-f)} \quad (4)$$

where r is the radius of the particle, $\Delta\alpha$ is the difference in the coefficient of the thermal expansion, ΔT is the difference between

the processing and test temperature. It is well known that, due to differences in the thermal expansion between SiC and Al matrix, rapid heating and cooling during USW increases the residual plastic strain and will lead to generation of dislocation at the matrix-SiC interface. In the BM region, the heating is much lower than the WZ. Therefore, there is a reduced driving force available to generate dislocation in the matrix of BM. Fourth, the Al_2Cu phase could be dissolved during USW and precipitated during following cooling process, which could also increase hardness of WZ. Several study of FSW of Al/SiC composite study shown the lower hardness in the WZ compare to that in BM [19]. Recently Uzun [20] for FSWed SiCp/AA2124 and Wang et al. [8] for FSWed SiCp/2009Al have studied the hardness profile across the welded region. It was found that the WZ has much lower hardness than that of the BM and further much lower in the HAZ region. It could be the because of the Al_2Cu (θ) and Al_2CuMg (S) phases became coarsen due to the longer welding cycle time in FSW. On the other hand, USW process duration is short, lead to slightly coarsen of precipitate particles. Therefore, hardness might not decrease significantly. This is the main creative of the study compared with FSW.

The reason behind the higher hardness in the 2000 J welded sample than that of the 1000 J one is that at higher welding energy, high frequency (20 kHz) ultrasonic vibration applies to the samples for longer period of time (1 s) leads higher temperature, thus more Al being squeezed off in 2000 J energy input sample. In the USWed SiC/2009Al-T6 composite sample, the average microhardness on the top and bottom of the specimens were measured around 180 HV, which is similar to that of BM (2009Al-T6/SiC). However, the higher hardness was not detected in the WZ region. But, it is worth to mention that the band region of USWed 2009Al-T6/SiC joint was much smaller ($\sim 60 \mu m$) than that ($\sim 1000 \mu m$) in USWed

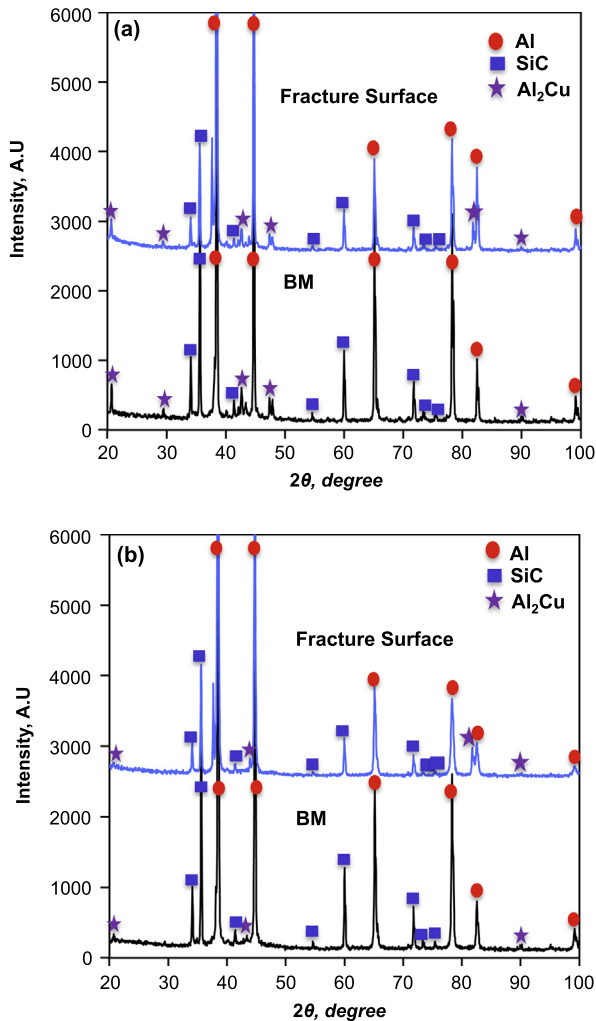


Fig. 5. XRD patterns obtained from the fracture surfaces of USW joints at a welding energy of 2000 J, (a) SiCp/2009Al-O and (b) SiCp/2009Al-T6.

2009Al-O/SiC (Figs. 2(b) and 3(b)). Thus, the impression of indentation encompass with small amount of band region during the microhardness test.

3.4. Lap shear tensile fracture load

As shown in Fig. 6(b), the maximum lap shear tensile load of USWed 2009Al-O/SiC and 2009Al-T6/SiC composites was 3.1 and 4.5 kN, respectively. It can be seen from that the samples fulfilled the AWS D17.2 standard [21] requirement for the spot weld, while the 2009Al-O/SiC samples at 2000 J energy input only 500 N away from the meeting the minimum requirement of AWS D17.2 standard [21]. The higher lap shear strength in the T6 condition samples is attributed to the higher strength hardening capacity of T6 samples compare to that of in O (annealing) samples. In both the USWed samples, the lap shear tensile load increased with increasing energy inputs and peaked 2000 J energy input. It can be seen from the images shown in Fig. 6(b) that lower energy samples (500–1000 J) experienced interfacial failure while higher energy samples (1500–2000) failed from the edge of NZ. This occurred because at lower energy inputs, the temperature was not high enough to soften or diffuse the Al matrix. On the other hand, higher welding energy values led to substantially higher temperatures and, the resulting softer Al sheet experiences a greater level of bending deformation in the weld zone compared

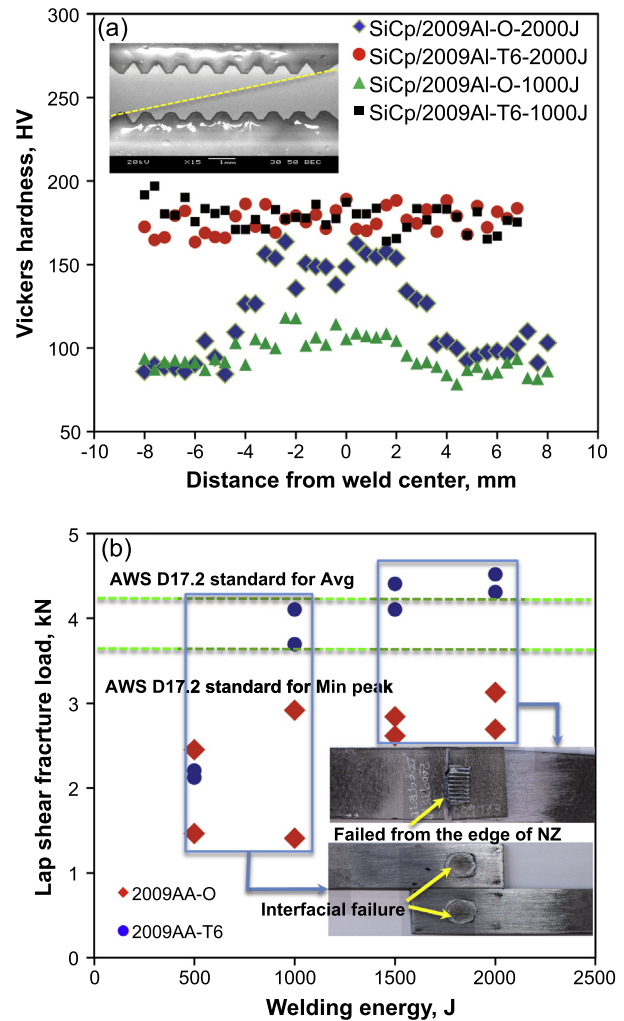


Fig. 6. (a) Microhardness profiles across the USWed 2009Al-O/SiC and 2009Al-T6/SiC at a welding energy of 1000 and 2000 J, (b) comparison of a lap shear fracture load of USWed SiCp/2009Al-O composite and SiCp/2009Al-T6 composite as a function of energy input.

with the base metal due to the outward flow of the material under the sonotrode tool indentation. This action of bending produced a small micro level crack at the notch of two sheets, and which previously observed in our previous study [22] and also in [23]. Finite element simulation showed that the normal tensile stress concentration at the periphery of the nugget could reach as high as more than five times the average stress under tensile-shear loading [23]. Thus, this micro level crack experienced higher stress concentration effect, which allowed the cracks to grow toward the outward Al sheet. Thus, the samples failed at the edge of the NZ (Fig. 6(b) failure location image). In this study, all composite samples (2009Al-O/SiC and 2009Al-T6/SiC) welded with 1500 J and more were failed at the edge of the NZ, while rest of the samples failed in the form of interfacial fracture (Fig. 6(b) failure location image).

4. Conclusions

USW of 1.5-mm thick SiCp/2009Al-O and SiCp/2009Al-T6 composites was successfully achieved. Both types of welded joints exhibited higher volume fractions of SiC particles in WZ, creating a distinctive band-like structure consisting of crushed fine SiC particles uniformly embedded in the aluminum matrix. This was mainly attributed to the squeeze-out effect of softer Al during

USW due to the severe shear strain rate caused by the high frequency vibration energy. The generation of θ phase during the aging process of parent metal was re-confirmed by XRD. The peaks of XRD showed that volume fraction of θ phase before and after welding remains same. The WZ of the joints had a much higher hardness than that of their respective base metal due to the presence of finer and denser crushed SiC particles. The 2000 J welded samples experienced higher hardness than that of 1000 J welded samples. This occurred because at higher welding energy, high frequency (20 kHz) ultrasonic vibration applies to the samples for longer period of time leads higher temperature, thus more Al being squeezed off in 2000 J energy input sample. The lap shear tensile fracture load increased as the welding energy increased, and the maximum lap shear tensile load of the USWed 2009Al–O/SiC and 2009Al–T6/SiC composites was obtained to be 3.1 and 4.5 kN, respectively, which fulfilled the requirements of AWS D17.2 standard. All lower energy samples (500–1000 J) experienced interfacial failure while higher energy samples (1500–2000 J) failed from the edge of NZ.

Acknowledgements

The authors would like to thank the Natural Sciences and Engineering Research Council of Canada (NSERC), AUTO21 Network of Centers of Excellence and National Basic Research Program of China (No. 2012CB619600) for providing financial support. One of the authors (D.L. Chen) is grateful for the financial support by the Premier's Research Excellence Award (PREA), NSERC-Discovery Accelerator Supplement (DAS) Award, Automotive Partnership Canada (APC), Canada Foundation for Innovation (CFI), and Ryerson Research Chair (RRC) program. The assistance of Q. Li, A. Machin, J. Amankrah, and R. Churaman in performing the experiments is gratefully acknowledged.

References

- [1] Wang D, Xiao BL, Wang QZ, Ma ZY. Friction stir welding of SiCp/2009Al composite plate. *Mater Des* 2013;47:243–7.
- [2] Ni DR, Chen DL, Wang D, Xiao BL, Ma ZY. Influence of microstructural evolution on tensile properties of friction stir welded joint of rolled SiCp/AA2009-T351 sheet. *Mater Des* 2013;51:199–205.
- [3] Xue C, Yu JK, Zhang ZQ. In situ joining of titanium to SiC/Al composites by low pressure infiltration. *Mater Des* 2013;47:267–73.
- [4] Clyne TW, Withers PJ. An introduction to metal matrix composites. UK: Cambridge University Press; 1993.
- [5] Bozkurt Y, Uzun H, Salman S. Microstructure and mechanical properties of friction stir welded particulate reinforced AA2124/SiC/25p-T4 composite. *J Compos Mater* 2011;45–21:2237–45.
- [6] Feng AH, Xiao BL, Ma ZY. Effect of microstructural evolution on mechanical properties of friction stir welded AA2009/SiCp composite. *Compos Sci Technol* 2008;68:2141–8.
- [7] Lee JA, Carter RW, Ding J. Friction stir welding for aluminum metal matrix composites (MMC's). NASA/TM (MSFC Center Director's Discretionary Fund Final Report, Project No. 98–09) 1999; 209876: 1–28.
- [8] Wang D, Wang QZ, Xiao BL, Ma ZY. Achieving friction stir welded SiCp/Al–Cu–Mg composite joint of nearly equal strength to base material at high welding speed. *Mater Sci Eng A* 2014;589:271–4.
- [9] Jahn R, Cooper R, Wilkosz D. The effect of anvil geometry and welding energy of microstructures in ultrasonic spot welds of AA6111-T4. *Metall Mater Trans A* 2007;38:570–83.
- [10] Hetrick E, Jahn R, Reatherford L, Skogsmo J, Ward S, Wilkosz D, et al. Ultrasonic spot welding: a new tool for aluminum joining. *Weld J* 2005:26–30.
- [11] Prangnell PB, Bakavos D. Novel approaches to friction spot welding thin aluminum automotive sheet. *Mater Sci Forum* 2010;638–642:1237–42.
- [12] Patel VK, Bhole SD, Chen DL. Improving weld strength of magnesium to aluminum dissimilar joints via tin interlayer during ultrasonic spot welding. *Sci Technol Weld Joining* 2012;17:342–7.
- [13] Bassani P, Capello E, Colombo D, Previtali B, Vedani M. Effect of process parameters on bead properties of A359/SiC MMCs welded by laser. *Composites Part A* 2007;38:1089–98.
- [14] Fan T, Zhang D, Shi Z, Wu R, Shibayangai T, Naka M, et al. The effect of Si upon the interfacial reaction characteristics in SiCp/Al–Si system composites during multiple-remelting. *J Mater Sci* 1999;34:5175–80.
- [15] Patel VK, Bhole SD, Chen DL. Influence of ultrasonic spot welding on microstructure in a magnesium alloy. *Scr Mater* 2011;65:911–4.
- [16] Elangovan S, Semeer S, Prakashan K. Temperature and stress distribution in ultrasonic metal welding—An FEA-based study. *J Mater Process Technol* 2009;209:1143–50.
- [17] Rodrigo P, Poza P, Utrilla MV, Ureña A. Identification of σ and Ω phases in AA2009/SiC composites. *J Alloys Compd* 2009;482–1–2:187–95.
- [18] Bakavos D, Prangnell PB. Mechanisms of joint and microstructure formation in high power ultrasonic spot welding 6111 aluminium automotive sheet. *Mater Sci Eng A* 2010;527:6320–34.
- [19] Yahya Bozkurt1, Hüseyin Uzun2, Serdar Salman. Microstructure and mechanical properties of friction stir welded particulate reinforced AA2124/SiC/25p–T4 composite. *J Compos Mater* 2011;45–21:2237–45.
- [20] Uzun H. Friction stir welding of SiC particulate reinforced AA2124. *Mater Des* 2007;28:1440–6.
- [21] AWS D 17.2. Specification for resistance welding for aerospace applications. American Welding Society; 2007.
- [22] Patel VK, Bhole SD, Chen DL. Ultrasonic spot welded AZ31 magnesium alloy: microstructure, texture, and lap shear strength. *Mater Sci Eng A* 2013;569:78–85.
- [23] Chang B, Shi Y, Liu L. Studies on the stress distribution and fatigue behavior of weld-bonded lap shear joints. *J Mater Process Technol* 2001;108:307–13.